© 2022. Published by The Company of Biologists Ltd | Development (2022) 149, dev200184. doi:10.1242/dev.200184

RESEARCH ARTICLE

The pseudobranch of jawed vertebrates is a mandibular arch-derived gill

Christine Hirschberger[1] and J. Andrew Gillis[1,2,*]

ABSTRACT

The pseudobranch is a gill-like epithelial elaboration that sits behind the jaw of most fishes. This structure was classically regarded as a vestige of the ancestral gill arch-like condition of the gnathostome jaw. However, more recently, hypotheses of jaw evolution by transformation of a gill arch have been challenged, and the pseudobranch has alternatively been considered a specialised derivative of the second (hyoid) pharyngeal arch. Here, we demonstrate in the skate (*Leucoraja erinacea*) that the pseudobranch does, in fact, derive from the mandibular arch, and that it shares gene expression features and cell types with gills. We also show that the skate mandibular arch pseudobranch is supported by a spiracular cartilage that is patterned by a *shh*-expressing epithelial signalling centre. This closely parallels the condition seen in the gill arches, where cartilaginous appendages called branchial rays, which support the respiratory lamellae of the gills, are patterned by a *shh*-expressing gill arch epithelial ridge. Together with similar discoveries in zebrafish, our findings support serial homology of the pseudobranch and gills, and an ancestral origin of gill arch-like anatomical features from the gnathostome mandibular arch.

KEY WORDS: Pseudobranch, Gill, Skate, Serial homology, Pharyngeal arch

INTRODUCTION

Hypotheses of jaw-gill arch serial homology are deeply rooted in the fields of vertebrate evolutionary biology and comparative anatomy, and have profoundly shaped views on the evolutionary origin of the jawed vertebrate body plan. Apparent correspondence between the upper and lower jaw and the dorsal (epibranchial) and ventral (ceratobranchial) segments of the gill arch skeleton was recognised over a century ago and has led to various scenarios of jaw evolution by transformation of an anterior member of a hypothetical primitive series of gill-bearing arches (e.g. Gegenbaur, 1878; De Beer, 1937; Jarvik, 1980; Mallatt, 1996). There is now very strong evidence of a shared transcriptional network underlying axial patterning of the mandibular, hyoid and gill arch skeletons of jawed vertebrates (Gillis et al., 2013; Takechi et al., 2013; Hirschberger et al., 2021; reviewed by Medeiros and Crump, 2012), with some features of this network predating the origin of jaws (Cerny et al., 2010; Kuraku et al., 2010; reviewed by Square et al., 2017). These findings are consistent with serial homology of distinct dorsal, ventral and intermediate domains of jawed vertebrate pharyngeal arches, and of the skeletal elements or tissues that derive, iteratively, from these domains.

The notion of an ancestral gill arch-like nature of the vertebrate mandibular arch, however, remains contentious on other grounds. Extant jawless vertebrates (i.e. cyclostomes – lampreys and hagfishes) do not have a gill associated with their mandibular arch derivatives, and in a rare instance of preservation of putative gill impressions in the pharyngeal region of a stem-vertebrate fossil, such impressions are apparently lacking from the anterior-most arch (Morris and Caron, 2014). Furthermore, the cyclostome mandibular arch gives rise to a velar skeleton that is morphologically distinct from the skeleton of the more caudal gill-bearing arches (Dohrn, 1882; Johnels, 1948), and there is indirect evidence that some stem-gnathostomes may have possessed a similar pharyngeal endoskeletal organisation (Janvier, 1996; Janvier, 1981, 1985a,b; Miyashita, 2016). Thus, in contrast to classical/neoclassical hypotheses of jaw origin by transformation of a gill arch, it has recently been suggested that the jaw instead evolved by 'mandibular confinement' of an ancestrally distinct and gill-less oral apparatus (Miyashita, 2016). According to this hypothesis, parallels in gnathostome jaw and gill arch skeletal organisation reflect secondary assimilation of the former to the latter, rather than retention of a primitive similarity.

Unlike cyclostomes, however, many jawed vertebrates do possess a gill-like epithelial elaboration called a 'pseudobranch' in close association with their mandibular arch derivatives. In teleost fishes, the pseudobranch resides in a subopercular cavity (Laurent and Dunel-Erb, 1984), while in most elasmobranch cartilaginous fishes (sharks, skates and rays) and in some non-teleost actinopterygian bony fishes (e.g. sturgeons, paddlefishes and bichirs), the pseudobranch resides within a spiracle – a small hole that opens behind the eye and that permits sustained water intake into the buccopharyngeal cavity while the mouth is buried in the substrate or is manipulating prey (Hughes, 1960) (Fig. 1A). During embryonic development, the spiracle forms by fusion of the first pharyngeal pouch with adjacent surface ectoderm and is therefore iteratively homologous with the gill slits that delineate the more-caudal hyoid and gill arches. Furthermore, in elasmobranchs, the pseudobranch is supported by a spiracular cartilage, which sits in the anterior wall of the spiracle (Fig. 1B,C). This spiracular cartilage has been homologised with the cartilaginous branchial rays that project into interbranchial septa from the epi- and ceratobranchials of the gill arches, and that support the respiratory lamellae of the gills (El-Toubi, 1947; Gillis et al., 2009a).

The close resemblance of the pseudobranch to the lamellae of the hyoid and gill arches, its location at the posterior margin of mandibular arch-derived structures and its formation, ancestrally,

[1]Department of Zoology, University of Cambridge, Downing Street, Cambridge CB2 3EJ, UK. [2]Marine Biological Laboratory, 7 MBL Street, Woods Hole, MA 02543, USA.

*Author for correspondence (jag93@cam.ac.uk)

J.A.G., 0000-0003-2062-3777

Handling Editor: Cassandra Extavour
Received 9 September 2021; Accepted 14 June 2022

Development (2022) 149, dev200184. doi:10.1242/dev.200184

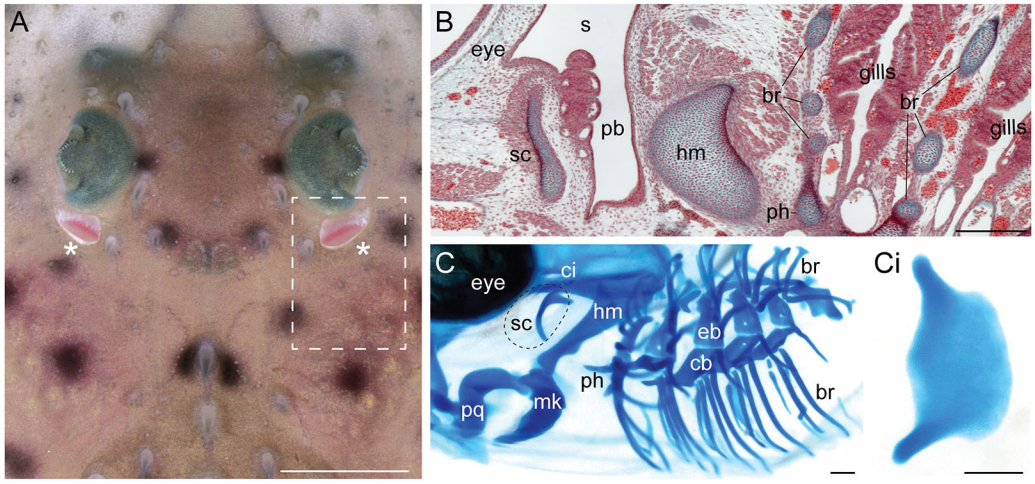

Fig. 1. Anatomical overview of the spiracle, pseudobranch and spiracular cartilage in the little skate. (A) Dorsal view of the eye and spiracle of a skate hatchling. The spiracles are indicated with asterisks. Dashed box indicates the regions shown in B and C. (B) Frontal section of a S32 skate embryo stained with Masson's trichrome showing the spiracular region. The pseudobranch sits inside the spiracle and is supported by the spiracular cartilage in the anterior spiracle wall. (C) Lateral view of a S32 skate embryo skeletal preparation stained with Alcian Blue showing the pharyngeal endoskeleton. The spiracular cartilage is located dorsal to the articulation between the upper jaw (palatoquadrate) and the lower jaw (Meckel's cartilage). (Ci) A dissected skate spiracular cartilage. The leaf-like sheet of cartilage supports the anterior wall of the spiracle. br, branchial rays; eb, epibranchials; hm, hyomandibula; mk, Meckel's cartilage; pb, pseudobranch; ph, pseudohyal; pq, palatoquadrate; s, spiracle; sc, spiracular cartilage. Scale bars: 3 cm in A; 500 µm in B-Ci.

within a gill slit serial homologue have led to its interpretation as a reduced or vestigial mandibular arch-derived gill (Mallatt, 1996). But the pseudobranch also exhibits some features that could be regarded as atypical of a gill, mandibular arch-derived or otherwise. For example, the pseudobranch is generally innervated by the facial (rather than trigeminal) nerve (Nilsson, 1984), and it receives oxygenated (rather than de-oxygenated) blood from the efferent hyoidean artery, via the afferent pseudobranchial artery (Hyrtl, 1838, as cited by Laurent and Dunel-Erb, 1984). For these reasons, it has been alternatively suggested that the pseudobranch is not a mandibular arch-derived gill, but rather is a specialised derivative of the second (hyoid) pharyngeal arch, which evolved to serve a non-respiratory, chemosensory function (Miyashita, 2016).

Patterns of serial homology may be recognised based on the apparent repetition or correspondence of anatomical features within an organism and are generally attributed to continuity or sharing of underlying developmental information (Van Valen, 1982; Roth, 1988; Wagner, 1989; Panchen, 1992). In many instances, serial homologues are arranged iteratively along the body, reflecting the serial repetition or re-deployment of a developmental mechanism along the embryonic axis (e.g. as with teeth, vertebrae, the paired appendages of jawed vertebrates or the wings and legs of arthropods; Van Valen, 1994; Ruvinsky and Gibson-Brown, 2000; Wagner, 2014; Bruce and Patel, 2020). But in some cases, serial homologues may arise by 'co-option' of developmental mechanisms and their deployment to spatially discontiguous locations within the body (e.g. as with the paired and median fins of jawed vertebrates; Freitas et al., 2006; Letelier et al., 2018). Importantly, serial homologues may be distinguished from structures within an organism that have converged on superficial anatomical similarity by their genesis via shared (whether iteratively or by co-option) or distinct developmental mechanisms, respectively (Hall, 2007). And while hypotheses of anatomical diversification of serial homologues over evolutionary time may be tested and falsified with palaeontological evidence, testing for shared developmental mechanisms as the basis of serial homology within extant taxa (and in the absence of fossil evidence) is inherently more difficult – the latter requiring a comparative analysis of embryonic context (e.g. tissue origin) and patterning mechanisms (e.g. tissue interactions, gene expression features and/or gene regulatory features), and ultimately an assessment of whether the weight of evidence points toward anatomical similarity arising via shared (i.e. conserved) or distinct generative pathways.

Here, we have investigated the nature and development of the pseudobranch in a cartilaginous fish, the skate *Leucoraja erinacea*. We demonstrate unequivocally, by histological and gene expression analyses and cell lineage tracing, that the skate pseudobranch is mandibular arch derived, and that it shares cell types and gene expression patterns with the gill lamellae of the hyoid and gill arches. We further show that the spiracular cartilage, which supports the pseudobranch in skate, is patterned by a *shh*-expressing epithelial signalling centre, in a manner that closely parallels the way in which hyoid and gill arch branchial rays are patterned by a *shh*-expressing gill arch epithelia ridge (GAER). Taken together, our findings strongly support the pseudobranch as a mandibular arch-derived gill serial homologue and, we argue, as a vestige of an ancestral gill arch-like nature of the vertebrate mandibular arch.

RESULTS

The skate pseudobranch is mandibular arch derived

In the skate, the developing pseudobranch is first apparent at S29 as a thickening of the epithelium of the posterior face of the mandibular arch (Fig. 2A), and by S30 we observe the first evidence of vasculature subjacent to this thickening (Fig. 2B). By early S31 (Fig. 2C), the pseudobranch is a gill lamella-like structure that extends into the spiracular cavity from the posterior face of the mandibular arch, and within the mandibular arch, we see condensation of the spiracular cartilage. The pseudobranch and spiracular cartilage continue to develop through later S31 (Fig. 2D), and by S32, these structures appear fully differentiated (Fig. 2E). Although the spiracular cartilage is closely associated with the palatoquadrate (Fig. 1), these elements condense and chondrify independently of one another (Fig. 2F-H).

Although the pseudobranch clearly appears to develop from the posterior face of the mandibular arch in the skate, we sought to directly confirm this embryonic origin by cell-lineage tracing. We and others have previously reported that *foxl2* is expressed in the

Development (2022) 149, dev200184. doi:10.1242/dev.200184

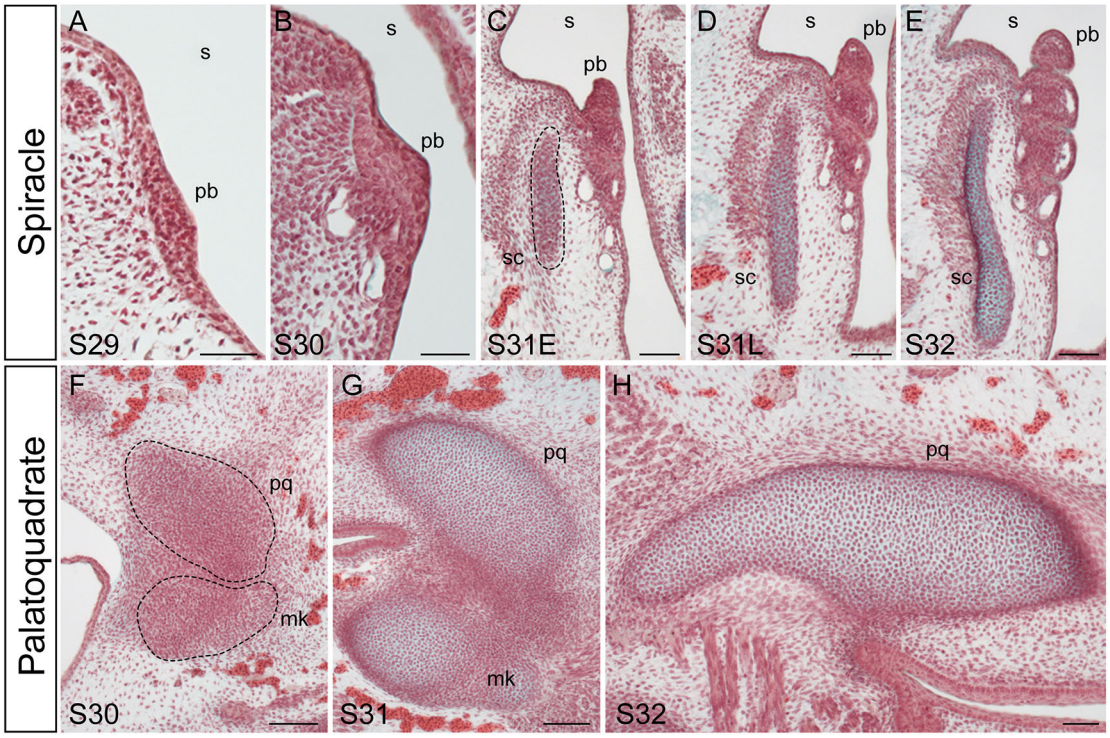

Fig. 2. Development of the pseudobranch, spiracular cartilage and palatoquadrate in the little skate. Frontal sections stained with modified Masson's trichrome. (A) At S29, the development of the pseudobranch is first apparent as a thickening of the posterior epithelium of the mandibular arch. (B) By S30, the pseudobranch thickens further and vasculature lies adjacent to it. (C,D) At S31, the pseudobranch extends from the posterior epithelium of the mandibular arch and takes on a lamellar-like morphology; the spiracular cartilage is condensing within subjacent mesenchyme (dashed line in C). (E) By S32, the pseudobranch and spiracular cartilage have fully differentiated. (F-H) The spiracular cartilage chondrifies completely independently of the condensing (F) and differentiating (G, H) palatoquadrate. mk, Meckel's cartilage; pb, pseudobranch; pq, palatoquadrate; s, spiracle; sc, spiracular cartilage. Scale bars: 50 µm.

core mesoderm and presumptive gill-forming epithelium of the pharyngeal arches of cartilaginous fishes (Wotton et al., 2007; Hirschberger et al., 2021). Analysis of *foxl2* expression by mRNA *in situ* hybridisation (ISH) in skate embryos at S24 reveals these expression patterns not only in the developing hyoid and gill arches, but also in the developing mandibular arch (Fig. 3A,B). We speculated that posterior mandibular arch epithelial expression of *foxl2* was serially homologous, with expression in the developing gill epithelium of the hyoid and gill arches, and that it marked the presumptive pseudobranch epithelium.

To test this, we broadly labelled the dorsal-intermediate mandibular arch in skate embryos at S23 with the lipophilic dye CM-DiI (Fig. 3C). At S23, the first pharyngeal endodermal pouch has fully fused with the surface ectoderm, permitting us to label mandibular arch tissues (both epithelium and underlying mesenchyme) broadly and specifically without risk of

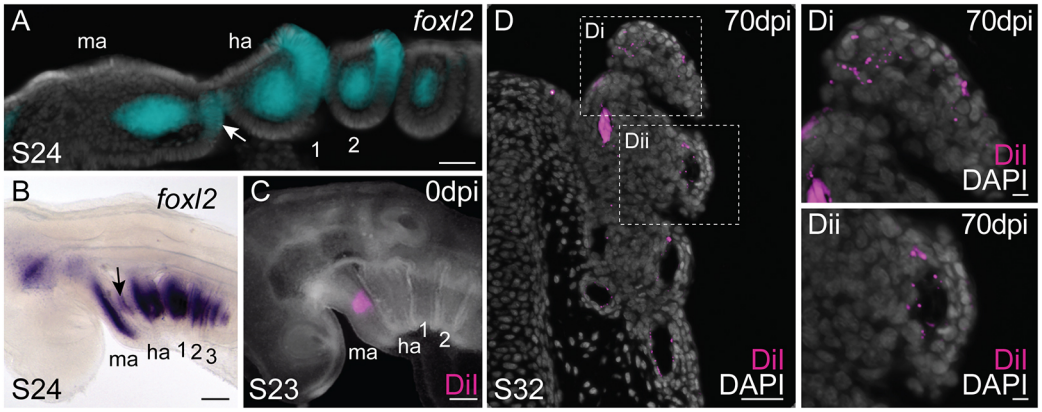

Fig. 3. The skate pseudobranch is mandibular arch derived. (A) mRNA *in situ* hybridisation for *foxl2*. At S24, *foxl2* is expressed in the mesodermal core of all pharyngeal arches, as well as in the presumptive pseudobranch epithelium of the mandibular arch (white arrow) and the presumptive gill epithelium of the hyoid and gill arches. (B) *foxl2*$^{+}$ presumptive pseudobranch epithelium (black arrow) is also apparent on the posterior mandibular arch following whole-mount mRNA *in situ* hybridisation. (C) Microinjection of the lipophilic dye CM-DiI in the posterior dorsal-intermediate mandibular arch of skate embryos at S23 broadly labels mandibular arch derivatives. (D) By S32 (after ~10 weeks of post-injection development), CM-DiI-positive cells are recovered throughout the skate pseudobranch, including (Di) within the lamellae of the pseudobranch as well as (Dii) in the walls of the pseudobranch vasculature. ha, hyoid arch; ma, mandibular arch; sc, spiracular cartilage; 1-3, gill arches 1-3. Scale bars: 50 µm A-D; 5 µm in Di,Dii.

Development (2022) 149, dev200184. doi:10.1242/dev.200184

contaminating the hyoid arch. Injected embryos were then reared until S32, by which point the pseudobranch has fully differentiated. Of 11 surviving embryos, nine retained CM-DiI-positive cells throughout the entirety of the pseudobranch (Fig. 3D). CM-DiI-positive cells were recovered throughout the pseudobranch lamellae (Fig. 3Di), as well as in the endothelial lining of the pseudobranch vasculature (Fig. 3Dii). No CM-DiI positive cells were recovered in any hyoid arch-derived features. These gene expression and lineage tracing findings conclusively demonstrate the mandibular arch origin of the pseudobranch in skate.

Conservation of gene expression between the skate pseudobranch and gill lamellae

The gill lamellae of bony fishes and cyclostomes possess neuroepithelial cells (NECs), which function to mediate physiological responses to hypoxia, and which are identifiable by their immunoreactivity for serotonin (5-HT) and synaptic vesicle glycoprotein 2 (SV2) (Dunel-Erb et al., 1982; Jonz and Nurse, 2003, 2005; Hockman et al., 2017). In skate gills at S32 (Fig. 4A), immunofluorescent detection of 5HT and SV2 confirms conservation of this putative hypoxia-sensitive neuroepithelial cell type in the tips of the gill lamellae (Fig. 4B-B-Biii). Using mRNA ISH, we also find that differentiated skate gill lamellae express the transcription factors *epas1/hif2a*, *gata2*, *gata3*, *gcm2* and *foxl2* (Fig. 4C-E; Fig. S1A,B), with *epas1/hif2a* expression likely reflecting cells that function in hypoxia sensitivity and/or stress response (Semenza, 2000; Dioum et al., 2009), and *gata2/gata3* and *gcm2* expression reflecting putative homology between the gills of fishes and the amniote parathyroid gland (Okabe and Graham, 2004).

Immunostaining and *in situ* hybridisation on sections revealed conservation of the above gene expression features in the skate pseudobranch (Fig. 4F). We found 5HT/SV2+ NECs in the tips of the pseudobranch lamellae (Fig. 4G-Giii), as well as pseudobranch expression of *hif2a*, *gata2*, *gata3*, *gcm2* and *foxl2* (Fig. 4H-J; Fig. S1C,D). These observations point to shared cell types and gene expression features – and, by extension, function – between the differentiated pseudobranch and gills of the skate, consistent with the serial homology of these structures.

Common origin of the skate spiracular cartilage and branchial rays from serially homologous domains of sonic hedgehog-responsive mesenchyme

The cartilaginous branchial rays that support the gill lamellae of the hyoid and gill arches of skates and sharks are patterned by a *shh*-expressing epithelial signalling centre called the gill arch epithelial ridge (GAER) (Gillis et al., 2009b, 2011; Gillis and Hall, 2016). In these arches, *shh* is initially broadly expressed in the posterior arch epithelium, and this expression then resolves into the GAER as the arches undergo a lateral expansion. Cell-lineage tracing has shown that branchial rays develop from GAER *shh*-responsive mesenchyme, and inhibition of GAER *shh* signalling results in a truncation/reduction of the branchial ray skeleton (Gillis et al., 2009b; Gillis and Hall, 2016).

We characterised *shh* expression in the developing mandibular arch of the skate. We found that, at S22, *shh* was broadly expressed in the posterior epithelium of the skate mandibular arch (Fig. 5A,B), with this expression resolving into a GAER-like ridge of *shh*-expressing cells along the posterior margin of the mandibular arch by S27 (Fig. 5C,D). This ridge of *shh* expression persisted into S29,

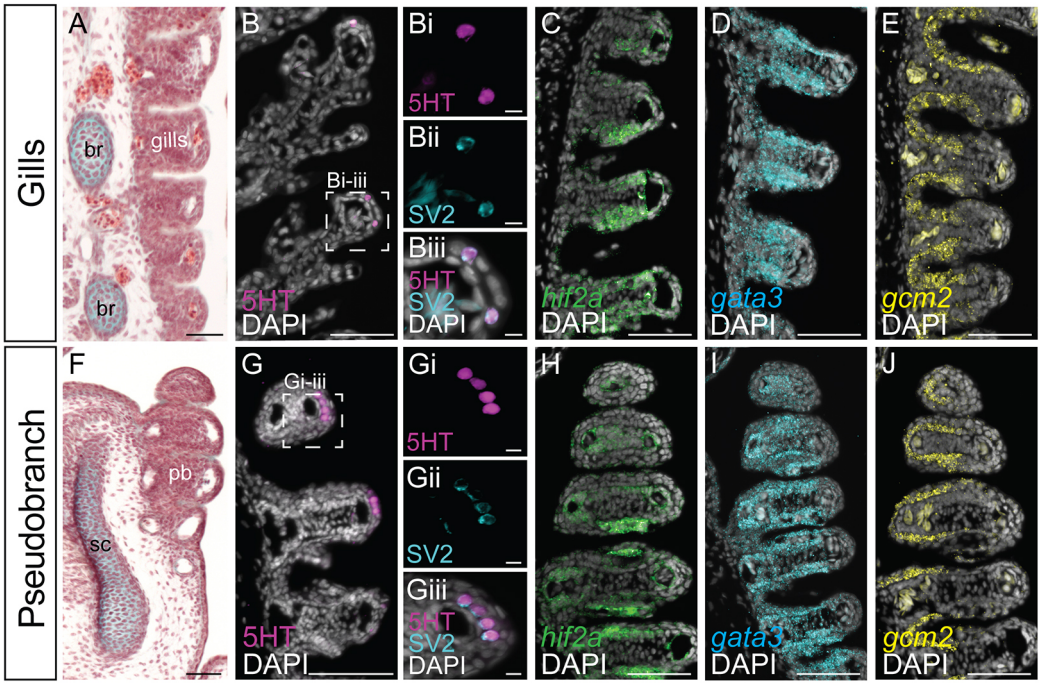

Fig. 4. Shared gene expression features of gills and the pseudobranch in skate. (A) In skate, interbranchial septa bearing gill lamellae are internally supported by cartilaginous branchial rays. Frontal section stained with modified Masson's trichrome. (B-Biii) Putative hypoxia-sensitive neuroepithelial cells (NECs) co-expressing serotonin and SV2 are present in S32 skate gill lamellae. Immunofluorescence on a frontal section. (C-E) Skate gills are marked by the expression of *hif2a* (C), *gata3* (D) and *gcm2* (E), as detected by mRNA in situ hybridisation by chain reaction on frontal sections. (F) The skate pseudobranch is internally supported by the spiracular cartilage. Frontal section stained with modified Masson's trichrome. (G-Giii) NECs co-expressing serotonin and SV2 are also present in the lamellae of the skate pseudobranch. Immunofluorescence on a frontal section. (H-J) The skate pseudobranch shares expression of *hif2a* (H), *gata3* (I) and *gcm2* (J) with gills, as detected by mRNA in situ hybridisation by chain reaction on frontal sections. br, branchial rays; sc, spiracular cartilage; pb, pseudobranch. Scale bars: 50 µm in A,B,C-E,F,G,H-J; 5 µm in Bi-Biii, Gi-Giii.

Development (2022) 149, dev200184. doi:10.1242/dev.200184

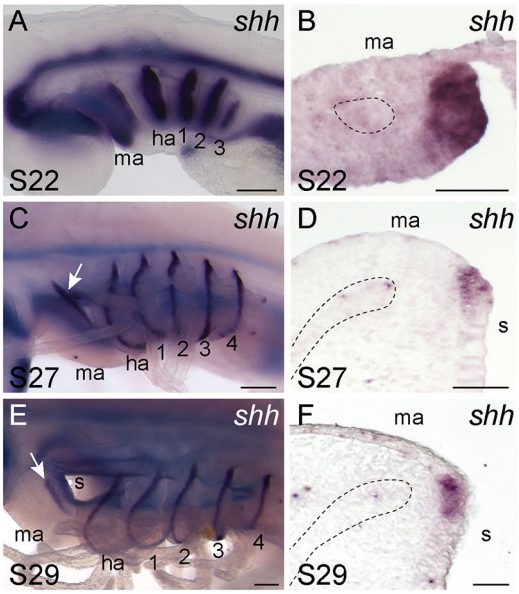

Fig. 5. A *shh*-expressing epithelial ridge on the skate mandibular arch. (A,B) At S22, *shh* is expressed broadly throughout the posterior epithelium of each pharyngeal arch in skate, including (B) the mandibular arch. (C,D) By S27, *shh* expression on the skate mandibular arch has resolved to a (D) thin ridge of cells lying along the posterior-lateral edge of the arch, comparable with the gill arch epithelial ridge (GAER) *shh* expression of the hyoid and gill arches reported by Gillis and Hall (2016). (E,F) At S29, *shh* persists in the mandibular hyoid and gill arch GAERs. A, C and E show whole-mount mRNA *in situ* hybridisation for *shh*. B, D and F show mRNA *in situ* hybridisation for *shh* on frontal sections through the mandibular arch. In B,D,F, the mesodermal core or muscle plate of the mandibular arch is outlined with a dashed line. ha, hyoid arch; ma, mandibular arch; 1-4, gill arches 1-4. Scale bars: 200 µm in A,C,E; 50 µm in B,D,F.

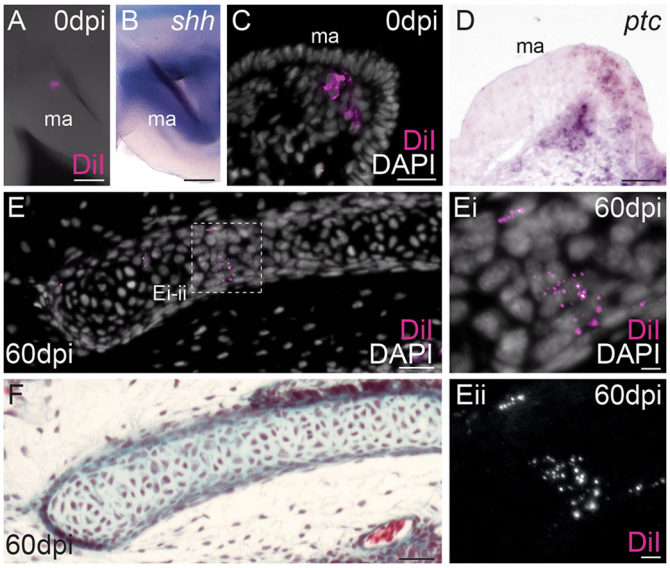

Fig. 6. The skate spiracular cartilage derives from GAER *shh*-responsive mandibular arch mesenchyme. (A-D) Microinjection of the lipophilic dye CM-DiI in the mandibular arch mesenchyme subjacent to the *shh*-expressing GAER (B) results in focal labelling of *ptc*+ (i.e. *shh* responsive) mesenchyme of the posterior mandibular arch (C,D). (E-F) At 60 days post-injection, CM-DiI-positive chondrocytes are recovered throughout the spiracular cartilage (F). ma, mandibular arch. Scale bars: 50 µm in A-E,F; 5 µm in Ei,Eii.

when it delineated the anterior edge of the spiracle (Fig. 5E,F). These patterns of *shh* expression in the mandibular arch are indistinguishable from the GAER *shh* expression of the branchial ray-bearing hyoid and gill arches, and led us to speculate about their possible skeletal patterning functions within the mandibular arch.

To test the fate of mesenchyme underneath the *shh*-expressing GAER of the skate mandibular arch, we labelled this tissue by microinjection of CM-DiI in skate embryos at S27 (Fig. 6A). We labelled *ptc*+ (*shh* responsive) mesenchymal cells underneath the mandibular arch GAER (Fig. 6B-D), reared injected embryos until S32 and then assessed the contribution of that tissue to the mandibular arch skeleton. Histological analysis of labelled embryos revealed CM-DiI-positive cells throughout the spiracular cartilage (Fig. 6E,F; Fig. S2; n=22/29), as well as in the connective tissue surrounding the spiracular cartilage. These experiments indicate that, like gill arch branchial rays, the spiracular cartilage develops from GAER *shh*-responsive mesenchyme of the mandibular arch.

The skate spiracular cartilage and branchial rays share *shh*-dependent patterning mechanisms

Finally, we set out to test whether mandibular arch GAER *shh* signalling patterns the spiracular cartilage in a manner that is comparable with the GAER patterning of hyoid and gill arch branchial rays. We have previously shown in skate that from S22 to S27, successively earlier inhibition of hedgehog signalling by cyclopamine treatment resulted in a progressively greater reduction of gill arch mesenchymal cell proliferation, and a corresponding reduction in the number of branchial rays on each arch (Gillis and Hall, 2016). To test the effects of hedgehog signalling inhibition on development of the spiracular cartilage, we conducted *in ovo* cyclopamine treatments with skate embryos at S22, S27 and S29, as per Gillis and Hall (2016), and assessed surviving embryos for spiracular cartilage defects at S32. Given the two-dimensional sheet-like nature of the skate spiracular cartilage, our test for spiracular cartilage reduction consisted of skeletal preparation, unilateral (left) spiracular cartilage dissection, measurement of spiracular cartilage area (standardised against total embryo length) and pairwise comparisons of mean ratios between control and cyclopamine-treated embryo at each stage.

Control (DMSO-treated) skate embryos showed no observable spiracular cartilage defects (Fig. 7A,A′), and spiracular cartilage area was not significantly different from wild-type S32 embryos (n=3, not shown). Conversely, cyclopamine treatment at S22 and S27 led to striking spiracular cartilage defects (Fig. 7B-C′), and to an overall significant reduction in spiracular cartilage area, relative to control (Fig. 7E). After treatment at S22, spiracular cartilages were either completely absent (n=3/6) or present as substantially reduced nodules of cartilage (n=3/6), while defects in embryos treated at S27 ranged from complete loss of the spiracular cartilage (n=2/12) to a reduction of the characteristic leaf-like sheet of cartilage, leaving only the slender endpoints connected by a thin bridge of cartilage (n=10/12). In contrast, cyclopamine treatment at S29 resulted in spiracular cartilages with some slightly abnormal morphology (Fig. 7D,D′), but no significant reduction in overall spiracular cartilage area relative to control (Fig. 7E). These findings reveal a shared role for GAER *shh* signalling in patterning the spiracular cartilage and branchial rays, and a shared period in development during which *shh* signalling is required for development of the spiracular cartilage and branchial rays.

DISCUSSION

Anatomical and histological similarities between the pseudobranch and gills are striking, and have led to hypotheses of their homology and, by extension, of an ancestral gill-bearing mandibular arch (Romer, 1970; Mallatt, 1996). The latter remains contentious,

Development (2022) 149, dev200184. doi:10.1242/dev.200184

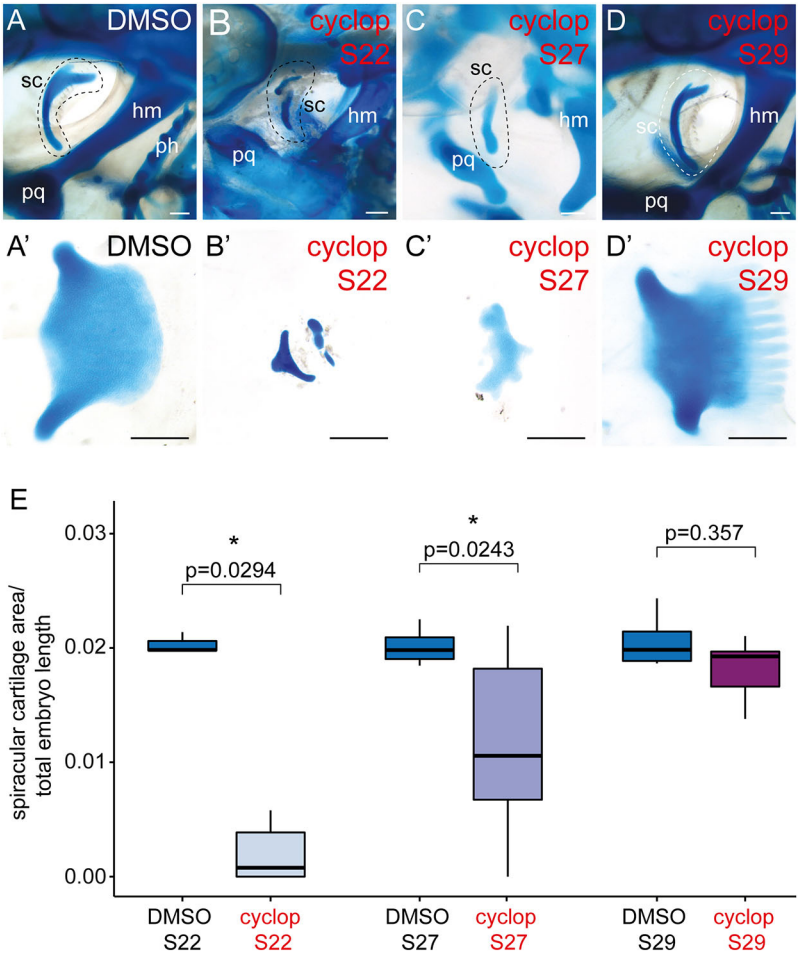

Fig. 7. Patterning of the skate spiracular cartilage by *shh* signalling. (A,C′) DMSO (control) treatment *in ovo* has no effect on spiracular cartilage morphology (A,A′), while treatment with 20 µM cyclopamine *in ovo* at S22 (B,B′) and S27 (C,C′) causes spiracular cartilage malformation and a reduction in spiracular cartilage size. (D,D′) Treatment with 20 µM cyclopamine *in ovo* at S29 has no significant effect on spiracular cartilage size. (E) Analysis of spiracular cartilage size (spiracular cartilage area/total embryo length) between cyclopamine- and DMSO-treated skate embryos at S22, S27 and S29 reveals statistically significant reductions in spiracular cartilage size with cyclopamine treatment at S22 and S27, but no significant reduction in spiracular cartilage size with cyclopamine treatment at S29. Kruskal–Wallis test followed by Dunn's test with Bonferroni correction. The horizontal lines represent the median, the boxes indicate the 1st and 3rd quantiles, and the whiskers indicate the maximum and minimum data points. hm, hyomandibula; ph, pseudohyal; pq, palatoquadrate; sc, spiracular cartilage. Scale bars: 500 µm.

owing to an absence of gill-like structures associated with mandibular arch derivatives in extant jawless vertebrates and to a lack of direct fossil evidence of the nature of first (mandibular) pharyngeal arch derivatives along the vertebrate and early gnathostome stems (Janvier, 1996; Miyashita, 2016). We have now presented unequivocal evidence for the mandibular arch origin of the pseudobranch in the skate, as well as developmental, gene expression and patterning similarities shared by the pseudobranch and gills (and, in the skate, their supporting skeletal elements). We argue that these similarities may only reasonably be interpreted as products of serial homology, with jawed vertebrates either retaining or atavistically re-evolving mandibular arch-derived gill structures that have been lost in extant cyclostomes, but that ancestrally formed iteratively from each pharyngeal arch (Fig. 8).

Vasculature, innervation and embryonic origin of the pseudobranch

It has been argued, based on irrigation with oxygenated blood from the efferent hyoidean artery and innervation by the facial nerve, that the pseudobranch of gnathostomes is not a derivative of the mandibular arch, but rather of the hyoid arch (Miyashita, 2016). We have shown that, in fact, the pseudobranch derives from a domain of *foxl2*-expressing epithelium on the posterior margin of the mandibular arch in skate (just as hyoid and gill lamellae derive from *foxl2*-expressing epithelial domains of their respective pharyngeal arches). However, regardless of this direct evidence of embryonic origin, the vascular and neural characteristics described above need not necessarily preclude a mandibular arch origin of the pseudobranch. In most fishes, blood supply to the afferent pseudobranchial artery does derive from the efferent hyoidean in adults, but this configuration arises from an embryonic pseudobranch vascular condition that more closely resembles that of the gills (Laurent and Dunel-Erb, 1984). For example, in shark embryos, the pseudobranch initially receives venous blood from the ventral aorta, with this connection subsequently degenerating as a novel blood supply from the afferent hyoidean artery is established secondarily (Scammon, 1911; De Beer, 1924; Daniel, 1934; Laurent and Dunel-Erb, 1984; Fig. S3). In addition, although mandibular arch-derived structures do tend to be innervated by the trigeminal nerve, there are exceptions: e.g. the maxillary barbels of teleosts develop from the mandibular arch but are innervated by the facial nerve (Kanwal et al., 1987; Caprio et al., 2015; LeClair and Topczewski, 2010; Moore et al., 2012). These observations underscore the difficulty of ascertaining embryonic origin based on adult innervation or vasculature, and the importance of direct embryonic observation and cell-lineage tracing for this purpose.

Conservation of pseudobranch and gill function

The gills of vertebrates function in gas exchange, ion homeostasis, chemoreception and excretion of nitrogenous waste (Evans et al., 2005; Fu et al., 2010). The pseudobranch is often referred to as a non-respiratory structure in adult fishes and, given its irrigation by oxygenated blood and its relatively small size, it does seem unlikely that the pseudobranch contributes significantly to blood gas exchange. However, the pseudobranch may function in gas exchange during the early life history stages of some teleost fishes (Dunel,

Development (2022) 149, dev200184. doi:10.1242/dev.200184

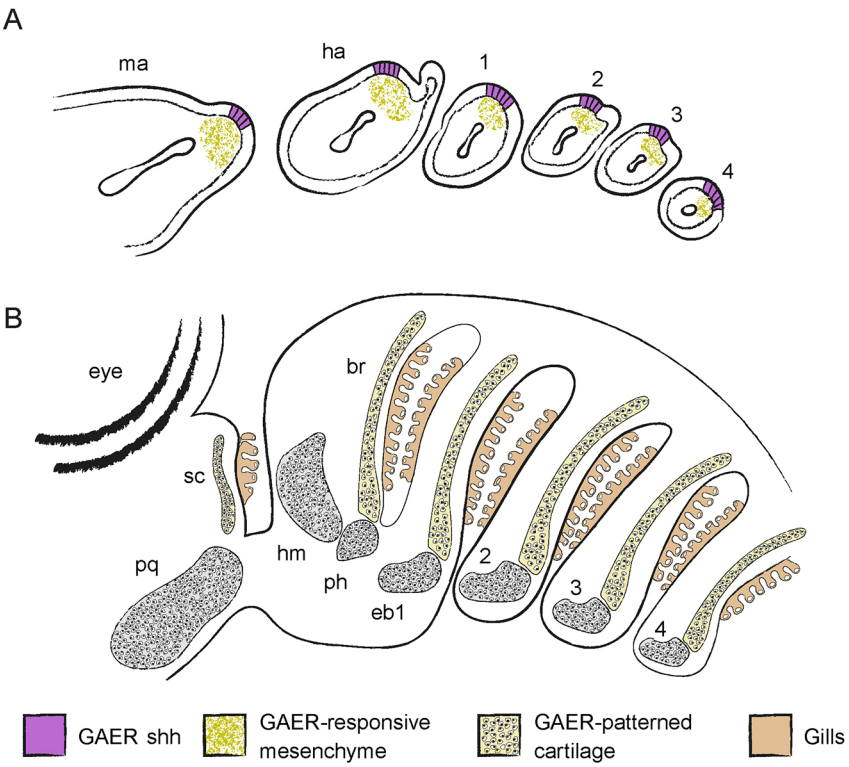

Fig. 8. Serial homology of the mandibular arch pseudobranch and spiracular cartilage with the gill alamellae and branchial rays in the little skate. (A) The mandibular, hyoid and gill arches of skate embryos each possess a *shh*-expressing gill arch epithelial ridge (GAER), which signals to underlying skeletogenic mesenchyme. These serially homologous signalling centres pattern the spiracular cartilage and branchial rays of the mandibular and hyoid/gill arches, respectively. (B) The spiracular cartilage and branchial rays serve to support the serially homologous pseudobranch (mandibular arch) and gill lamellae (hyoid and gill arches), respectively. br, branchial rays; eb1-4, epibranchials 1-4; ha, hyoid arch; hm; hyomandibula; ma, mandibular arch; ph, pseudohyal; pq, palatoquadrate; sc, spiracular cartilage.

1975; Laurent and Dunel-Erb, 1984). Given the remodelling of pseudobranch vasculature that occurs through ontogeny (see above), it seems plausible that the non-respiratory role of this structure reflects an evolutionary reduction following relaxed constraint and changing function of mandibular arch derivatives, rather than an independent origin of the pseudobranch, to fulfil a physiological role distinct from that of the gills.

Indeed, our gene expression analyses lend support to hypotheses of a generally shared function between gills and the pseudobranch. In tetrapods, GATA transcription factors function upstream of *Gcm2* to specify cells of the parathyroid gland, an endodermally derived structure that functions in regulating extracellular calcium homeostasis (Kim et al., 1998; Günther et al., 2000; Gordon et al., 2001; Liu et al., 2007; Grigorieva et al., 2010). In fishes, this function is performed by the gills, which are also endodermally derived (Warga and Nusslein-Volhard, 1999; Gillis and Tidswell, 2017; Hockman et al., 2017), express *gcm2* and are generally regarded as homologues of the tetrapod parathyroid gland (Okabe and Graham, 2004). Our *in situ* gene expression data for *gata2*, *gata3* and *gcm2* indicate conservation of this function not only in the gills, but also in the mandibular arch pseudobranch. Additionally, the gills of fishes contain hypoxia-sensitive, chemoreceptive neuroepithelial cells (NECs), recognisable based on their morphology and co-expression of 5HT and SV2 (Dunel-Erb et al., 1982; Jonz & Nurse, 2003, 2005; Hockman et al., 2017). These cells are dispersed throughout gill lamellae, are sensitive to acute changes in partial pressure of oxygen and elicit behavioural changes (e.g. increased breathing frequency and amplitude) to match oxygen supply to metabolic demand (reviewed by Milsom, 2012). Consistent with physiological evidence for a shared chemoreceptive function of the pseudobranch and gills (Laurent and Rouzeau, 1972), we find in skate that both contain 5HT/SV2+ putative hypoxia-sensitive NECs. Thus, contrary to arguments that the pseudobranch performs chemosensory or osmoregulatory functions that are distinct from those of the gills, our gene expression data are consistent with previous physiological studies in pointing to a broad conservation of pseudobranch and gill function in fishes.

Serial homology of the spiracular cartilage and branchial rays of elasmobranch fishes

Each of the hyoid and gill arches of sharks, skates and rays is associated with a series of paired, cartilaginous appendages called branchial rays (Gillis et al., 2009b). These appendages articulate proximally with the epi- and ceratobranchial components of the arches, and project distally into interbranchial septa, where they serve as attachment points for branchiomeric musculature and support the respiratory lamellae of the gills. Branchial rays arise as discrete condensations that are distinct from their associated gill arch cartilages and develop under the influence of a *shh*-expression epithelial signalling centre called the gill arch epithelial ridge (GAER): *shh* signalling maintains proliferation of branchial ray progenitors, and progressively earlier inhibition of hedgehog signalling with the small molecule antagonist cyclopamine results in a successively greater reduction of the branchial ray series (Gillis and Hall, 2016). In cartilaginous fishes, the pseudobranch of the mandibular arch is supported by one or more spiracular cartilages that form in close association with the palatoquadrate (upper jaw). In sharks, spiracular cartilages occur as multiple flattened rods that splay or bifurcate distally, while in skates the spiracular cartilage forms as a continuous sheet of cartilage (El-Toubi, 1947). It has been suggested that the spiracular cartilage could represent a mandibular arch homologue of the hyoid and gill arch branchial rays (Gegenbaur, 1872; El-Toubi, 1947; Holmgren and Stensiö, 1936; El-Toubi, 1947) or, alternatively, a separate otic process of the palatoquadrate, which condenses as an extension of palatoquadrate, but then subsequently separates and chondrifies as a distinct element (Huxley, 1876; Parker, 1878; Edgeworth, 1925).

We find in skate that the spiracular cartilage condenses and chondrifies completely independently of the palatoquadrate, in a

Development (2022) 149, dev200184. doi:10.1242/dev.200184

temporal and spatial configuration that parallels that of the branchial ray and gill arch cartilages. Moreover, we find that the spiracular cartilage develops beneath a *shh*-expressing GAER on the mandibular arch, from *shh*-responsive (i.e. *ptc*-expressing) mesenchyme, and that progressively earlier inhibition of hedgehog signalling with cyclopamine results in a successively greater reduction of the spiracular cartilage. These mandibular arch signalling interactions and spiracular cartilage phenotypes precisely mirror those of the hyoid and gill arch GAERs and branchial rays, and we therefore argue that the former are clear serial homologues of the latter (Fig. 5).

To date, branchial rays and spiracular cartilages have only been resolved to the chondrichthyan stem (Gillis et al., 2011; Burrow et al., 2020), and there is little fossil evidence of the presence of these features outside chondrichthyans. Spiracles are often difficult to interpret in the fossil record. Some placoderms possessed an opening in the position of a spiracle (Young and Zhang, 1992; Arsenault et al., 2004), but distinguishing this feature from other gaps in their heavy dermal armour remains challenging. It is similarly challenging to reconstruct the internal anatomy of the spiracular region from fossils, although some have described grooves in stem gnathostome and stem osteichthyan skulls that may represent remnants of the efferent pseudobranchial artery (Goodrich, 1930; Gardiner, 1984; Basden et al., 2000). A notable exception is the Middle Devonian acanthodiform *Cheiracanthus murchisoni* (Burrow et al., 2020). *Cheiracanthus* possessed a spiracular skeleton that takes the form of both rods and a flattened element in each spiracle, possibly forming a valve for controlled water flow over the pseudobranch. The series of thin parallel rods associated with the *Cheiracanthus* spiracular skeleton bears a strong resemblance to branchial rays and is more reminiscent of the rod-like spiracular cartilage of extant sharks than the sheet-like spiracular cartilage found in skate. *Cheiracanthus* may thus represent a transitional state between an ancestral gnathostome mandibular arch condition, with a less constrained first gill slit and a gill arch-like mandibular arch, and the derived condition of extant elasmobranchs bearing spiracles with a reduced pseudobranch and supporting spiracular skeleton.

Conclusions

Most questions of body plan evolution may be framed as hypotheses of historical or serial homology – that is, homology of structures across or within taxa, respectively. Hypotheses of historical homology aim to resolve the polarity of character state changes on an evolutionary timescale by considering corresponding features within a phylogenetic context, while hypotheses of serial homology attempt to explain anatomical similarity due to shared underlying developmental mechanisms (Wagner, 1989, 1994). But while hypotheses of serial homology may be formulated based on observation of anatomy or development even in a single taxon, such hypotheses must ultimately incorporate phylogeny, in order to distinguish between serial homology with ancestral polyisomery (repeated units that were ancestrally similar) or ancestral anisomery (repeated units that were ancestrally dissimilar, but that acquire a derived or secondary similarity) (Miyashita and Diogo, 2016).

The evolutionary history of the vertebrate mandibular arch remains obscure, owing to a dearth of fossils showing direct evidence of endoskeletal and/or soft tissue anatomy at the origin of jaws. We are therefore left in the somewhat difficult position of weighing limited, indirect evidence of ancestral mandibular arch anatomy and function from fossils against the striking anatomical and developmental similarities between the mandibular and gill arches of some extant taxa. We can now confidently infer that a gill-like pseudobranch is an ancestral feature of the gnathostome mandibular arch, based on our findings here and on parallel work in zebrafish, which demonstrates a mandibular arch origin of the pseudobranch as well as shared gene expression features, cis-regulatory elements and *gata3* dependence with gills (Thiruppathy et al., 2022). A spiracular cartilage and branchial rays, on the other hand, can (at present) only be resolved to the chondrichthyan stem. Although it has been suggested that some stem-gnathostomes possessed a non-respiratory mandibular arch, possibly resembling, the oral apparatus of extant cyclostomes, more recent palaeontological evidence points instead to the ancestral presence of a complete spiracular gill between the mandibular and hyoid arches at the base of the gnathostome stem (Gai et al., 2022). We suggest that the conserved, iterative development of the pseudobranch and gill lamellae of the mandibular, hyoid and gill arches (and, in chondrichthyans, their supporting skeletons) is too precisely similar in terms of embryology, gene expression and function to be attributable to convergent evolution, and that secondary co-option of a gill developmental programme to the mandibular arch need not be invoked. Rather, we speculate that these similarities reflect an ancestral and deeply conserved gill arch-like nature of the gnathostome (if not vertebrate) mandibular arch, and that the pseudobranch of extant fishes is a vestige of this ancestral gill arch-like condition.

MATERIALS AND METHODS

Embryo collection and fate mapping

All animal work complied with protocols approved by the Institutional Animal Care and Use Committee at the Marine Biological Laboratory (MBL; Woods Hole, MA, USA). Skate (*Leucoraja erinacea*) eggs were obtained from the Marine Resources Centre of the MBL. Staging was carried out according to Maxwell et al. (2008) and Ballard et al. (1993). Embryos for histological and gene expression analyses were fixed in 4% paraformaldehyde (PFA) in 1× phosphate-buffered saline (PBS) overnight at 4°C, then rinsed in 1× PBS, dehydrated into methanol and stored in methanol at −20°C prior to analysis. Embryos for cell-lineage tracing experiments were maintained in a flow-through seawater system at ∼15°C. For CM-DiI (ThermoFisher) labelling of the mandibular arch at S22, eggs were windowed and microinjection of the mandibular arch with CM-DiI was performed *in ovo* according to Gillis and Tidswell (2017). For labelling of the mandibular arch at S27, embryos were removed from the egg and anaesthetised in a petri dish of seawater containing 10 mg/ml ethyl 3-aminobenzoate methanesulfonate salt (MS-222, Sigma) prior to microinjection, according to Gillis and Hall (2016). CM-DiI-injected embryos were left to develop for 6-10 weeks, and then fixed in 4% PFA in PBS overnight at 4°C, rinsed three times in PBS and stored at 4°C in PBS with 0.01% sodium azide before analysis.

Paraffin embedding and sectioning

All embryos for paraffin histology were dehydrated into 100% ethanol (or changed from 100% methanol to 100% ethanol) before clearing in Histosol (National Diagnostics). Embryos were washed three times for 20 min each in Histosol at room temperature, twice for 30 min each in 1:1 Histosol: paraffin at 60°C and then then moved into molten paraffin wax for overnight at 60°C. The following day, embryos were washed four times for 1 h each in paraffin, and then embedded in peel-a-way moulds. Embedded embryos were sectioned at 8 µm on a Leica RM2125 rotary microtome and sections were mounted on Superfrost Plus slides (Fisher). Histochemical staining was performed using the modified Masson's trichrome staining protocol of Witten and Hall (2003).

mRNA *in situ* hybridisation and immunofluorescence

Chromogenic mRNA *in situ* hybridisation for *foxl2* (MW457610), *gata2* (MZ501824), *shh* (EF100667) and *ptc* (EF100663) was performed in

Development (2022) 149, dev200184. doi:10.1242/dev.200184

wholemount as described by Hirschberger et al. (2021), and on paraffin wax-embedded sections as described by O'Neill et al. (2007) with modifications according to Gillis et al. (2012). mRNA *in situ* hybridisation by chain reaction on paraffin wax-embedded sections was carried out according to Choi et al. (2018), with modifications as described by Criswell and Gillis (2020). Probe sets against *Leucoraja erinacea hif2a/epas1* (MZ501826; MI lot no. PRH337), *gata3* (MZ501825; MI lot no. PRJ403) and *gcm2* (MW389327; MI lot no. PRJ404), and HCR amplification hairpins were purchased from Molecular Instruments (https://www.molecularinstruments.com). Slides to be used for immunofluorescence were dewaxed in histosol and rehydrated through a descending ethanol series into 1×PBS+0.1% Triton X-100 (PBT). For antigen retrieval, slides were preheated in distilled water for 5 min at 60°C, transferred to prewarmed antigen retrieval solution (10 mM sodium citrate at pH 6.0) and incubated for 25 min at 95°C. Slides were then cooled at −20°C for 30 min. Slides were rinsed three times for 10 min each in PBT, blocked for 30 min in 10% sheep serum and incubated in primary antibody under a parafilm coverslip in a humidified chamber overnight at 4°C. The next day, slides were rinsed three times for 5 min each in PBT and incubated in secondary antibody under a parafilm coverslip in a humidified chamber overnight at 4°C. Slides were then rinsed three times for 10 min each in PBT and coverslipped with Fluoromount G containing DAPI (Southern Biotech). Primary and secondary antibodies were diluted as follows: rabbit anti-5HT (Merck S5545, 1:250); mouse anti-SV2 (Developmental Studies Hybdridoma Bank, 1:100); goat anti-rabbit 488 (ThermoFisher A11008, 1:500); and goat anti-mouse 633 (ThermoFisher A21050, 1:500).

In ovo cyclopamine treatment, whole-mount skeletal preparation and statistical analysis

In ovo cyclopamine treatment was performed according to Gillis and Hall (2016). Briefly, skate eggs have an approximate internal chamber volume of 12 ml. To achieve an *in ovo* cyclopamine concentration of ∼20 µM, 25 µl of 9 mM stock solution of cyclopamine (LC labs) in dimethylsulfoxide (DMSO) was injected into skate eggs at S22, S27 or S29, using a syringe and 30-gauge needle. For control embryos, an equivalent volume of DMSO was injected into the egg. Cyclopamine-treated embryos were grown to S32, and surviving embryos (n=6/21, n=12/28 and n=7/19 for cyclopamine treatment at S22, S27 and S29, respectively, and n=3/3, n=4/5 and n=5/5 for DMSO control treatment at S22, S27 and S29, respectively) were fixed as described above and analysed for skeletal defects by skeletal preparation.

For whole-mount staining of the endoskeleton, skate embryos were moved from 100% methanol into 70% ethanol at room temperature. Embryos were then stained with 0.2 mg/ml Alcian Blue 8GX (Sigma) in acetic ethanol (3:7 glacial acetic acid: absolute ethanol) for 24 h with gentle rocking at room temperature. Embryos were destained in acetic ethanol for 24 h, rehydrated through a descending ethanol series, washed in double distilled water, and digested in 1% w/v trypsin in 2% w/v sodium tetraborate for 20 min. Embryos were then cleared in a graded 0.5% w/v KOH:glycerol series (3:1, 1:1, 1:3 0.5% KOH:glycerol) for 24 h/step. Specimens were stored in 80% glycerol at 4°C and manually dissected for photography.

For the statistical analysis, the dissected left spiracular cartilage of each embryo was imaged on a Leica M165FC stereomicroscope, and the surface area of each cartilage was measured using Fiji (Schindelin et al., 2012) and normalised against embryo total length. To test for statistically significant differences among the means of normalised spiracular cartilage area for each group (DMSO at S22, cyclopamine at S22, DMSO at S27, cyclopamine at S27, DMSO at S29 and cyclopamine at S29), a Kruskal–Wallis analysis of variance was performed, followed by a Dunn's test with Bonferroni correction to identify which pairwise comparisons were statistically significantly different. The same statistical analysis confirmed no significant difference between normalised spiracular cartilage area of DMSO-treated versus wild-type (n=3) spiracular cartilages at S32 (P=0.305).

Acknowledgements

We thank Dr Richard Schneider, Prof. David Sherwood and the Marine Biological Laboratory Embryology course for provision of lab space; Louise Bertrand and Leica Microsystems for microscopy support; and David Remsen, Scott Bennett, Dan Calzarette and staff of the Marine Biological Laboratory Marine Resources Center for technical and animal husbandry assistance. We also thank Dr Kate Criswell, Dr Vicky Sleight, Jenaid Rees, Dr Kate Rawlinson, the University of Cambridge chordate evo-devo community and Dr Carole Burrow for helpful discussion. Some of the text and figures in this paper formed part of Marie Christine Hirschberger's PhD thesis in Zoology at Downing College, University of Cambridge in March 2021.

Competing interests

The authors declare no competing or financial interests.

Author contributions

Conceptualization: J.A.G.; Methodology: J.A.G.; Formal analysis: C.H., J.A.G.; Investigation: C.H., J.A.G.; Writing - original draft: C.H.; Writing - review & editing: C.H., J.A.G.; Supervision: J.A.G.; Project administration: J.A.G.; Funding acquisition: J.A.G.

Funding

This work was supported by a Biotechnology and Biological Sciences Research Council Doctoral Training Partnership studentship to C.H., and by a Royal Society University Research Fellowship (UF130182 and URF\R\191007), a Royal Society Research Fellows Enhancement Award (RGF/EA/180087) and a University of Cambridge Sir Isaac Newton Trust Grant (14.23z) to J.A.G. Open access funding provided by the University of Cambridge. Deposited in PMC for immediate release.

Peer review history

The peer review history is available online at https://journals.biologists.com/dev/article-lookup/doi/10.1242/dev.200184

References

Arsenault, M., Desbiens, S., Janvier, P. and Kerr, J. (2004). New data on the soft tissues and external morphology of the antiarch *Bothriolepis canadensis* (Whiteaves, 1880), from the Upper Devonian of Miguasha, Québec. In *Recent Advances in the Origin and Early Radiation of Vertebrates* (ed. G. Arratia, M. C. H. Wilson and R. Cloutier), pp. 439-454. Munich: Verlag Dr. Friedrich Pfeil.

Ballard, W. W., Mellinger, J. and Lechenault, H. (1993). A series of normal stages for development of *Scyliorhinus canicula*, the lesser spotted dogfish (Chondrichthyes: Scyliorhinidae). *J. Exp. Zool.* **267**, 318-336. doi:10.1002/jez.1402670309

Basden, A. M., Young, G. C., Coates, M. I. and Ritchie, A. (2000). The most primitive osteichthyan braincase? *Nature* **403**, 185-188. doi:10.1038/35003183

Bruce, H. S. and Patel, N. H. (2020). Knockout of crustacean leg patterning genes suggests that insect wings and body walls evolved from ancient leg segments. *Nat. Ecol. Evol.* **4**, 1703-1712. doi:10.1038/s41559-020-01349-0

Burrow, C. J., Newman, M. J. and den Blaauwen, J. L. (2020). First evidence of a functional spiracle in stem chondrichthyan acanthodians, with the oldest known elastic cartilage. *J. Anat.* **236**, 1154-1159. doi:10.1111/joa.13170

Caprio, J., Shimohara, M., Marui, T., Kohbara, J., Harada, S. and Kiyohara, S. (2015). Amino acid specificity of fibers of the facial/trigeminal complex innervating the maxillary barbel in the Japanese sea catfish, *Plotosus japonicus*. *Physiol. Behav.* **152**, 288-294. doi:10.1016/j.physbeh.2015.10.011

Cerny, R., Cattell, M., Sauka-Spengler, T., Bronner-Fraser, M., Yu, F. and Medeiros, D. M. (2010). Evidence for the prepattern/cooption model of vertebrate jaw evolution. *Proc. Natl Acad. Sci. USA* **107**, 17262-17267. doi:10.1073/pnas.1009304107

Choi, H. M. T., Schwarzkopf, M., Fornace, M. E., Acharya, A., Artavanis, G., Stegmaier, J., Cunha, A. and Pierce, N. A. (2018). Third-generation *in situ* hybridization chain reaction: multiplexed, quantitative, sensitive, versatile, robust. *Development* **145**, dev165753. doi:10.1242/dev.165753

Criswell, K. E. and Gillis, J. A. (2020). Resegmentation is an ancestral feature of the gnathostome vertebral skeleton. *Elife* **9**, e51696. doi:10.7554/eLife.51696

Daniel, J. F. (1934). *The Elasmobranch Fishes*, 3rd edn. Berkeley: University of California Press.

De Beer, G. R. (1924). Memoirs: studies on the vertebrate head: part I. Fish. *J. Cell. Sci.* **s2-68**, 287-341. doi:10.1242/jcs.s2-68.270.287

De Beer, G. R. (1937). *The Development of the Vertebrate Skull*. Oxford: Clarendon.

Dioum, E. M., Chen, R., Alexander, M. S., Zhang, Q., Hogg, R. T., Gerard, R. D. and Garcia, J. A. (2009). Regulation of hypoxia-inducible factor 2α signaling by the stress-responsive deacetylase sirtuin 1. *Science* **324**, 1289-1293. doi:10.1126/science.1169956

Dohrn, A. (1882). Studien zur Urgeschichte des Wirbelthierkörpers. *Mittheilungen aus der Zoologischen Station zu Neapal* **4**, 172-190.

Dunel, S. (1975). Contribution à l'étude structurale et ultrastructurale de la pseudobranchie et de son innervation chez les Téléostéens. PhD Thesis, University of Strasbourg, France.

Dunel-Erb, S., Bailly, Y. and Laurent, P. (1982). Neuroepithelial cells in fish gill primary lamellae. *J. Appl. Physiol.* **53**, 1342-1353. doi:10.1152/jappl.1982.53.6.1342
Edgeworth, F. H. (1925). On the autostylism of Dipnoi and Amphibia. *J. Anat.* **59**, 225-264.
El-Toubi, M. R. (1947). The development of the spiracular cartilages of the spiny dogfish, *Acanthias vulgaris*. *Biol. Bull.* **93**, 287-295. doi:10.2307/1537977
Evans, D. H., Piermarini, P. M. and Choe, K. P. (2005). The multifunctional fish gill: dominant site of gas exchange, osmoregulation, acid-base regulation, and excretion of nitrogenous waste. *Physiol. Rev.* **85**, 97-177. doi:10.1152/physrev.00050.2003
Freitas, R., Zhang, G. J. and Cohn, M. J. (2006). Evidence that mechanisms of fin development evolved in the midline of early vertebrates. *Nature* **442**, 1033-1037. doi:10.1038/nature04984
Fu, C., Wilson, J. M., Rombough, P. J. and Brauner, C. J. (2010). Ions first: Na^+ uptake shifts from the skin to the gills before O_2uptake in developing rainbow trout. *Oncorhynchus mykiss*. *Proc. R. Soc. B Biol. Sci.* **277**, 1553-1560. doi:10.1098/rspb.2009.1545
Gai, Z., Zhu, M., Ahlberg, P. E. and Donoghue, P. C. J. (2022). The evolution of the spiracular region from jawless fishes to tetrapods. *Front. Ecol. Evol.* **10**, 887172. doi:10.3389/fevo.2022.887172
Gardiner, B. G. (1984). The relationships of the palaeoniscoid fishes, a review based on new specimens of *Mimia* and *Moythomasia* from the Upper Devonian of Western Australia. *Bull. Br. Mus. Nat. Hist. Geol.* **37**, 173-428.
Gegenbaur, C. (1872). *Untersuchungen zur vergleichenden Anatomie der Wirbelthiere. III. Das Kopfskelet der Selachier.* Leipzig: Wilhelm Engelmann.
Gegenbaur, C. (1878). *Elements of Comparative Anatomy*. London: MacMillan and Co.
Gillis, J. A. and Hall, B. K. (2016). A shared role for sonic hedgehog signalling in patterning chondrichthyan gill arch appendages and tetrapod limbs. *Development* **143**, 1313-1317. doi:10.1242/dev.133884
Gillis, J. A. and Tidswell, O. R. A. (2017). The origin of vertebrate gills. *Curr. Biol.* **27**, 729-732. doi:10.1016/j.cub.2017.01.022
Gillis, J. A., Dahn, R. D. and Shubin, N. H. (2009a). Chondrogenesis and homology of the visceral skeleton in the little skate, *Leucoraja erinacea* (*Chondrichthyes: Batoidea*). *J. Morphol.* **270**, 628-643. doi:10.1002/jmor.10710
Gillis, J. A., Dahn, R. D. and Shubin, N. H. (2009b). Shared developmental mechanisms pattern the vertebrate gill arch and paired fin skeletons. *Proc. Natl. Acad. Sci. USA* **106**, 5720-5724. doi:10.1073/pnas.0810959106
Gillis, J. A., Rawlinson, K. A., Bell, J., Lyon, W. S., Baker, C. V. H. and Shubin, N. H. (2011). Holocephalan embryos provide evidence for gill arch appendage reduction and opercular evolution in cartilaginous fishes. *Proc. Natl. Acad. Sci. USA* **108**, 1507-1512. doi:10.1073/pnas.1012968108
Gillis, J. A., Modrell, M. S., Northcutt, R. G., Catania, K. C., Luer, C. A. and Baker, C. V. H. (2012). Electrosensory ampullary organs are derived from lateral line placodes in cartilaginous fishes. *Development* **139**, 3142-3146. doi:10.1242/dev.084046
Gillis, J. A., Modrell, M. S. and Baker, C. V. H. (2013). Developmental evidence for serial homology of the vertebrate jaw and gill arch skeleton. *Nat. Commun.* **4**, 1436. doi:10.1038/ncomms2429
Goodrich, E. S. (1930). *Studies on the Structure and Development of Vertebrates.* London: Macmillan.
Gordon, J., Bennett, A. R., Blackburn, C. C. and Manley, N. R. (2001). Gcm2 and Foxn1 mark early parathyroid-and thymus-specific domains in the developing third pharyngeal pouch. *Mech. Dev.* **103**, 141-143. doi:10.1016/S0925-4773(01)00333-1
Grigorieva, I. V., Mirczuk, S., Gaynor, K. U., Nesbit, M. A., Grigorieva, E. F., Wei, Q., Ali, A., Fairclough, R. F., Stacey, J. M., Stechman, M. J. et al. (2010). Gata3-deficient mice develop parathyroid abnormalities due to dysregulation of the parathyroid-specific transcription factor Gcm2. *J. Clin. Invest.* **120**, 2144-2155. doi:10.1172/JCI42021
Günther, T., Chen, Z. F., Kim, J., Priemel, M., Rueger, J. M., Amling, M., Moseley, J. M., Martin, T. J., Anderson, D. J. and Karsenty, G. (2000). Genetic ablation of parathyroid glands reveals another source of parathyroid hormone. *Nature* **406**, 199-203. doi:10.1038/35018111
Hall, B. K. (2007). Homoplasy and homology: dichotomy or continuum? *J. Hum. Evol.* **52**, 473-479. doi:10.1016/j.jhevol.2006.11.010
Hirschberger, C., Sleight, V. A., Criswell, K. E., Clark, S. J. and Gillis, J. A. (2021). Conserved and unique transcriptional features of pharyngeal arches in the skate (*Leucoraja erinacea*) and evolution of the jaw. *Mol. Biol. Evol.* **38**, 4187-4204. doi:10.1093/molbev/msab123
Hockman, D., Burns, A. J., Schlosser, G., Gates, K. P., Jevans, B., Mongera, A., Fisher, S., Unlu, G., Knapik, E. W., Kaufman, C. K. et al. (2017). Evolution of the hypoxia-sensitive cells involved in amniote respiratory reflexes. *Elife* **6**, e21231. doi:10.7554/eLife.21231
Holmgren, N. and Stensiö, E. (1936). Kranium und visceralskelett der acranier, cyclostonien und fische. *Bolk Handb. verg. Anat. Berlin* **4**.
Hughes, G. M. (1960). The mechanism of gill ventilation in the dogfish and skate. *J. Exp. Biol.* **37**, 11-27. doi:10.1242/jeb.37.1.11
Huxley, T. H. (1876). 8. Contributions to morphology. Ichthyopsida. No 1. On *Ceratodus forsteri*, with observations on the classification of fishes. *Proc. Zool. Soc. Lond.* **1876**, 24-59. doi:10.1111/j.1096-3642.1876.tb02541.x
Hyrtl, J. (1838). Beobachtungen aus dem gebiete der vergleichenden gefässlehre. 11. Uber den bau der kiemen der fische. *Med. Jahrb.* **15**, 232-248.
Janvier, P. (1981). *Norselaspis glacialis* n.g., n.sp. et les relations phylogénétiques entre les Kiaeraspidiens (Osteostraci) du Dévonien inféerieur du Spitsberg. *Palaeovertebrata* **11**, 19-131.
Janvier, P. (1985a). *Les Céphalaspides du Spitsberg. Anatomie, phylogénie et systématique des Ostéostracés siluro-dévoniens. Révision des Ostéostracés de la Formation de Wood Bay (Dévonien inférieur du Spitsberg).* Cahiers de Paléontologie. Paris: Centre national de la Recherche scientifique.
Janvier, P. (1985b). Les Thyestidiens (Ostéostraci) du Silurien de Saaremaa (Estonie). Première partie: morphologie et anatomie. *Ann. Paléontol.* **71**, 83-147.
Janvier, P. (1996). *Early Vertebrates*. Oxford: Clarendon.
Jarvik, E. (1980). *Basic Structure and Evolution of Vertebrates*. London: Academic Press.
Johnels, A. G. (1948). On the development and morphology of the skeleton of the head of *Petromyzon*. *Acta Zool.* **29**, 139-279. doi:10.1111/j.1463-6395.1948.tb00030.x
Jonz, M. G. and Nurse, C. A. (2003). Neuroepithelial cells and associated innervation of the zebrafish gill: a confocal immunofluorescence study. *J. Comp. Neurol.* **461**, 1-17. doi:10.1002/cne.10680
Jonz, M. G. and Nurse, C. A. (2005). Development of oxygen sensing in the gills of zebrafish. *J. Exp. Biol.* **208**, 1537-1549. doi:10.1242/jeb.01564
Kanwal, J. S., Hidaka, I. and Caprio, J. (1987). Taste responses to amino acids from facial nerve branches innervating oral and extra-oral taste buds in the channel catfish, *Ictalurus punctatus*. *Brain Res.* **406**, 105-112. doi:10.1016/0006-8993(87)90774-8
Kim, J., Jones, B. W., Zock, C., Chen, Z., Wang, H., Goodman, C. S. and Anderson, D. J. (1998). Isolation and characterization of mammalian homologs of the Drosophila gene glial cells missing. *Proc. Natl. Acad. Sci. USA* **95**, 12364-12369. doi:10.1073/pnas.95.21.12364
Kuraku, S., Takio, Y., Sugahara, F., Takechi, M. and Kuratani, S. (2010). Evolution of oropharyngeal patterning mechanisms involving Dlx and endothelins in vertebrates. *Dev. Biol.* **341**, 315-323. doi:10.1016/j.ydbio.2010.02.013
Laurent, P. and Dunel-Erb, S. (1984). The Pseudobranch: morphology and function. *Fish Physiol.* **10**, 285-323. doi:10.1016/S1546-5098(08)60188-0
Laurent, P. and Rouzeau, J. D. (1972). Afferent neural activity from pseudobranch of teleosts. Effects of PO2, pH, osmotic pressure and Na+ ions. *Respir. Physiol.* **14**, 307-331. doi:10.1016/0034-5687(72)90037-0
LeClair, E. E. and Topczewski, J. (2010). Development and regeneration of the zebrafish maxillary barbel: a novel study system for vertebrate tissue growth and repair. *PLoS One* **5**, e8737. doi:10.1371/journal.pone.0008737
Letelier, J., de la Calle-Mustienes, E., Pieretti, J., Naranjo, S., Maeso, I., Nakamura, T., Pascual-Anaya, J., Shubin, N. H., Schneider, I., Martinez-Morales, J. R. et al. (2018). A conserved Shh cis-regulatory module highlights a common developmental origin of unpaired and paired fins. *Nat. Genet.* **50**, 504-509. doi:10.1038/s41588-018-0080-5
Liu, Z., Yu, S. and Manley, N. R. (2007). *Gcm2* is required for the differentiation and survival of parathyroid precursor cells in the parathyroid/thymus primordia. *Dev. Biol.* **305**, 333-346. doi:10.1016/j.ydbio.2007.02.014
Mallatt, J. (1996). Ventilation and the origin of jawed vertebrates: a new mouth. *Zool. J. Linnean Soc.* **117**, 329-404. doi:10.1111/j.1096-3642.1996.tb01658.x
Maxwell, E. E., Fröbisch, N. B. and Heppleston, A. C. (2008). Variability and conservation in late chondrichthyan development: ontogeny of the winter skate (*Leucoraja Ocellata*). *Anat. Rec.* **291**, 1079-1087. doi:10.1002/ar.20719
Medeiros, D. M. and Crump, J. G. (2012). New perspectives on pharyngeal dorsoventral patterning in development and evolution of the vertebrate jaw. *Dev. Biol.* **371**, 121-135. doi:10.1016/j.ydbio.2012.08.026
Milsom, W. K. (2012). New insights into gill chemoreception: receptor distribution and roles in water and air breathing fish. *Respir. Physiol. Neurobiol.* **184**, 326-339. doi:10.1016/j.resp.2012.07.013
Miyashita, T. (2016). Fishing for jaws in early vertebrate evolution: a new hypothesis of mandibular confinement. *Biol. Rev.* **91**, 611-657. doi:10.1111/brv.12187
Miyashita, T. and Diogo, R. (2016). Evolution of serial patterns in the vertebrate pharyngeal apparatus and paired appendages via assimilation of dissimilar units. *Front. Ecol. Evol.* **4**, 71. doi:10.3389/fevo.2016.00071
Moore, A. C., Mark, T. E., Hogan, A. K., Topczewski, J. and LeClair, E. E. (2012). Peripheral axons of the adult zebrafish maxillary barbel extensively remyelinate during sensory appendage regeneration. *J. Comp. Neurol.* **520**, 4184-4203. doi:10.1002/cne.23147
Morris, S. C. and Caron, J.-B. (2014). A primitive fish from the Cambrian of North America. *Nature* **512**, 419-422. doi:10.1038/nature13414
Nilsson, S. (1984). Innervation and pharmacology of the gills. *Fish Physiol.* **10**, 185-227. doi:10.1016/S1546-5098(08)60319-2
Okabe, M. and Graham, A. (2004). The origin of the parathyroid gland. *Proc. Natl. Acad. Sci. USA* **101**, 17716-17719. doi:10.1073/pnas.0406116101

O'Neill, P., McCole, R. B. and Baker, C. V. H. (2007). A molecular analysis of neurogenic placode and cranial sensory ganglion development in the shark, *Scyliorhinus canicula*. *Dev. Biol.* **304**, 156-181. doi:10.1016/j.ydbio.2006.12.029
Panchen, A. L. (1992). *Classification, Evolution, and the Nature of Biology*. Cambridge: Cambridge University Press.
Parker, W. K. (1878). On the structure and development of the skull in sharks and skates. *Trans. Zool. Soc. Lond.* **10**, 189-234. doi:10.1111/j.1096-3642.1878.tb00286.x
Romer, A. S. (1970). *The Vertebrate Body*. Philadelphia: Saunders.
Roth, V. L. (1988). The biological basis of homology. In *Ontogeny and Systematics* (ed. C.J. Humphries), pp. 1-26. New York: Columbia University Press.
Ruvinsky, I. and Gibson-Brown, J. J. (2000). Genetic and developmental bases of serial homology in vertebrate limb evolution. *Development* **127**, 5233-5244. doi:10.1242/dev.127.24.5233
Scammon, R. E. (1911). Normal plates of the development of *Squalus acanthias*. In *Normentafeln zur Entwicklungsgeschichts der Wirbeltiere*, Vol. 12 (ed. G. Fischer), pp. 1-140. Gustav Fischer Verlag.
Schindelin, J., Arganda-Carreras, I., Frise, E., Kaynig, V., Longair, M., Pietzsch, T., Preibisch, S., Rueden, C., Saalfeld, S., Schmid, B. et al. (2012). Fiji: an open-source platform for biological-image analysis. *Nat. Methods* **9**, 676-682. doi:10.1038/nmeth.2019
Semenza, G. L. (2000). HIF-1: mediator of physiological and pathophysiological response to hypoxia. *J. Appl. Physiol.* **88**, 1474-1480. doi:10.1152/jappl.2000.88.4.1474
Square, T., Jandzik, D., Romášek, M., Cerny, R. and Medeiros, D. M. (2017). The origin and diversification of the developmental mechanisms that pattern the vertebrate head skeleton. *Dev. Biol.* **427**, 219-229. doi:10.1016/j.ydbio.2016.11.014
Takechi, M., Adachi, N., Hirai, T., Kuratani, S. and Kuraku, S. (2013). The Dlx genes as clues to vertebrate genomics and craniofacial evolution. *Sem. Cell Dev. Biol.* **24**, 110-118. doi:10.1016/j.semcdb.2012.12.010
Thiruppathy, M., Fabian, P., Gillis, J. A. and Crump, J. G. (2022). Gill developmental program in the teleost mandibular arch. *eLife* **11**, e78170. doi:10.7554/eLife.78170
Van Valen, L. (1982). Homology and causes. *J. Morphol.* **173**, 305-312. doi:10.1002/jmor.1051730307
Van Valen, L. (1994). Serial homology: the crests and cusps of mammalian teeth. *Acta. Palaeontol. Pol.* **38**, 145-158.
Wagner, G. P. (1989). The biological homology concept. *Annu. Rev. Ecol. Evol. Syst.* **20**, 51-69. doi:10.1146/annurev.es.20.110189.000411
Wagner, G. P. (1994). Homology and the mechanisms of development. In *Homology: The Hierarchical Basis of Comparative Biology* (ed. B. K. Hall), pp. 273-299. London: Academic Press.
Wagner, G. P. (2014). *Homology, Genes and Evolutionary Innovation*. Princeton: Princeton University Press.
Warga, R. M. and Nusslein-Volhard, C. (1999). Origin and development of the zebrafish endoderm. *Development* **126**, 827-838. doi:10.1242/dev.126.4.827
Witten, P. E. and Hall, B. K. (2003). Seasonal changes in the lower jaw skeleton in male Atlantic salmon (*Salmo salar* L.): remodelling and regression of the kype after spawning. *J. Anat.* **203**, 435-450. doi:10.1046/j.1469-7580.2003.00239.x
Wotton, K. R., French, K. E. and Shimeld, S. M. (2007). The developmental expression of *foxl2* in the dogfish *Scyliorhinus canicula*. *Gene Expr. Patterns* **7**, 793-797. doi:10.1016/j.modgep.2007.05.003
Young, G. C. and Zhang, G. (1992). Structure and function of the pectoral joint and operculum in antiarchs, Devonian placoderm fishes. *Palaeontology* **35**, 443-464.

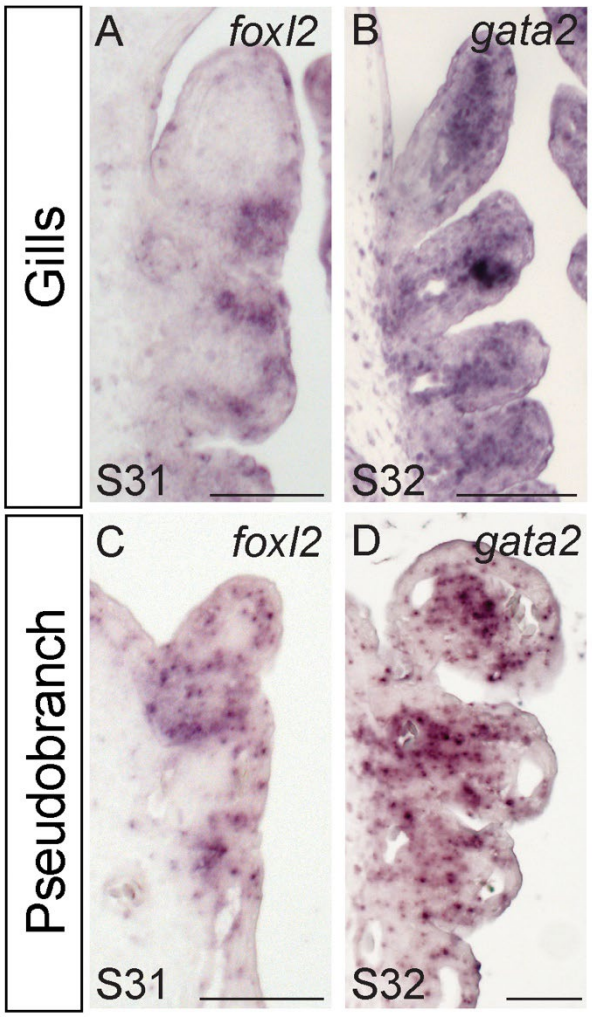

Fig. S1. Additional shared gene expression features of the gills and pseudobranch of the skate. (A) Expression of *foxl2* and **(B)** *gata2* in the gills of the skate. **(C)** Expression of *foxl2* and **(D)** *gata2* in the pseudobranch of the skate. Scale bars: 50µm.

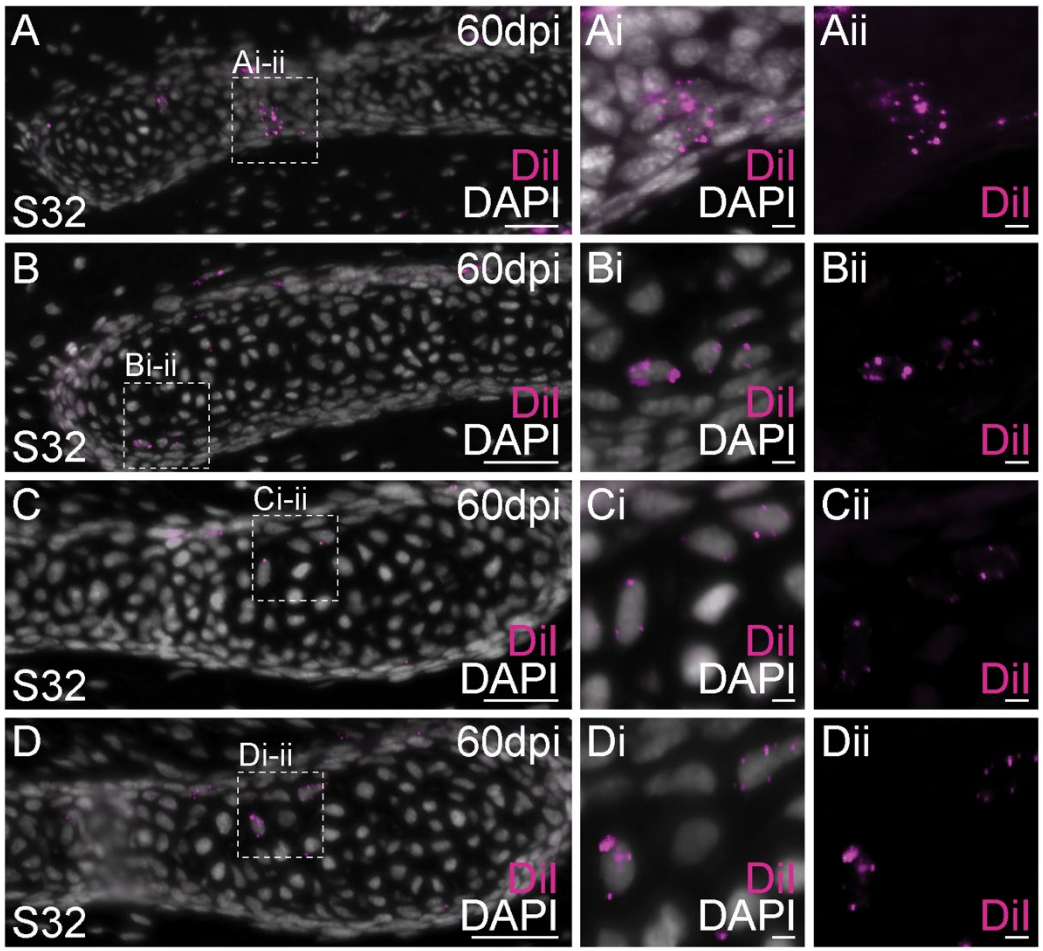

Fig. S2. Additional examples of CM-DiI-labelled chondrocytes, derived from mandibular arch GAER shh-responsive mesenchyme, in the skate spiracular cartilage. Scale bars: A-D=50µm, Ai/Aii-Di/Dii=5µm.

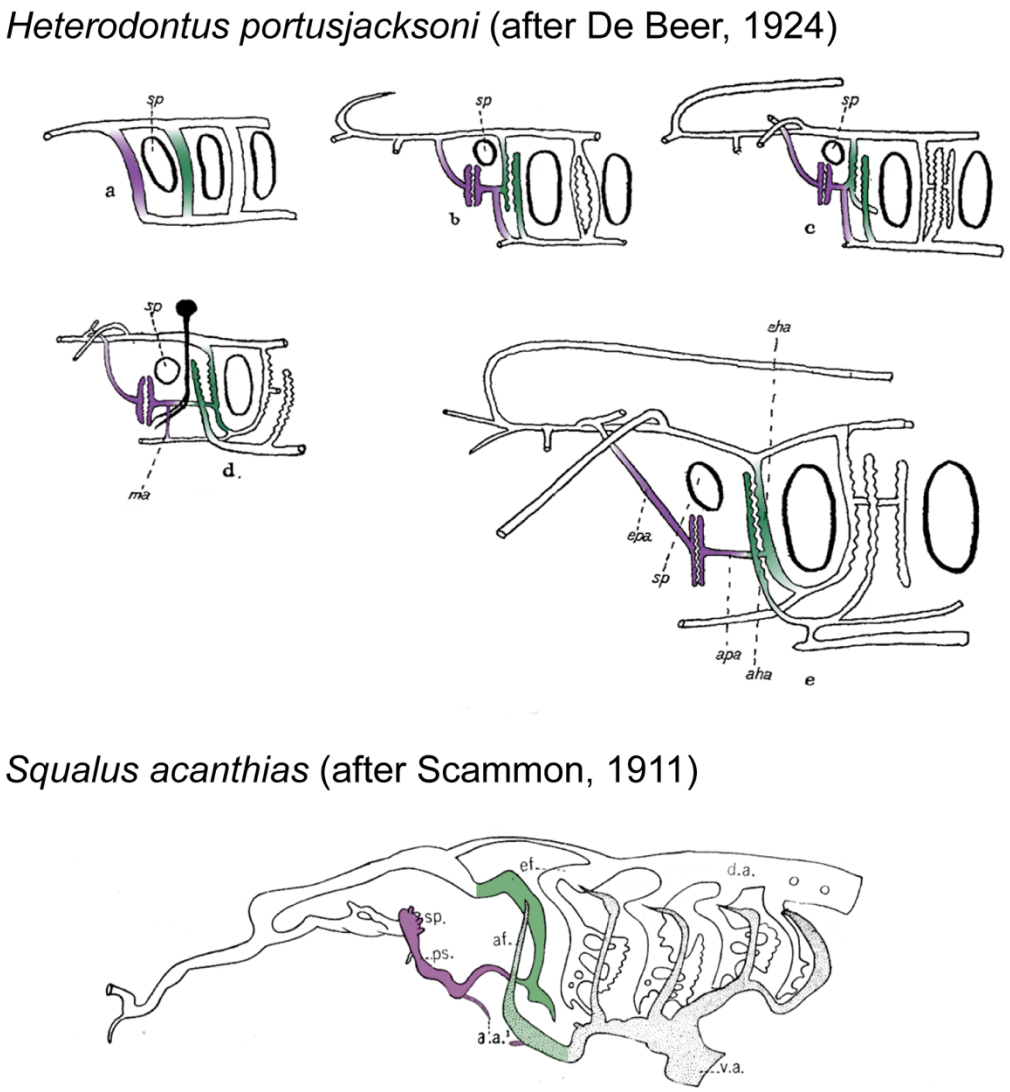

Fig. S3. Development and remodelling of pseudobranch vasculature in *Heterodontus portusjacksoni* and *Squalus acanthias*. At the top of the figure, embryological investigation of vasculature in *H. portusjacksoni* embryos after De Beer (1924). In **(a)**-**(e)**, mandibular arch vasculature is coloured purple, and hyoid arch vasculature is coloured green. **(a)** In an 11mm *H. portusjacksoni* embryo, the dorsal and ventral aorta are connected by distinct mandibular and hyoid arch blood vessels. **(b)** At 21mm, the spiracular hemibranch (future pseudobranch) has formed, the mandibular arch vessel has split into efferent and afferent pseudobranchial artery, and the hyoid arch vessel has split into efferent and afferent hyoidean arteries. The afferent pseuobranchial artery connects with the ventral aorta and, via a cross commissure, with the efferent hyoidean artery. **(c)** This vascular configuration persists at 25mm, and by **(d)** 45mm, the connection between the afferent pseudobranchial artery and the ventral aorta begins to breakdown. At this stage,

the remnant of the mandibular artery and the efferent hyoidean artery no longer communicate with the ventral aorta, and instead join the rudiment of the hypobranchial artery. **(e)** By 70mm, the remnant of the mandibular artery is gone, and the afferent pseudobranchial artery receives only oxygenated blood from the cross commissure with the efferent hyoidean artery. Selected abbreviations from the original paper: *aha*, afferent hyoidean artery; *apa*, afferent pseudobranchial artery; *eha*, efferent hyoidean artery; *epa*, efferent pseudobranchial artery; *ma*, mandibular artery; *sp*, spiracle. At the bottom of the figure, an image of embryonic cranial vasculature of *S. acanthias* by Scammon (1911). The pseudobranchial artery (purple) receives blood only from the efferent hyoidean artery (green), and remnants (a.a[1]) of the recently degraded connection between the pseudobranchial artery and the ventral aorta are still visible. Selected abbreviations from the original paper: *af*, afferent hyoidean artery; *da*, dorsal aorta; *ef*, efferent hyoidean artery; *ps*, pseudobranchial artery; *sp*, spiracle; *va*, ventral aorta.